ARTICLES

X-ray-absorption spectroscopy and x-ray diffraction in discontinuous Co_xFe_{1-x}/Ag multilayers

W. H. Flores, S. R. Teixeira, and J. B. M. da Cunha
Instituto de Física–UFRGS, Caixa Postal 15051, 91501-970 Porto Alegre, Brazil

M. C. Martins Alves and H. Tolentino
Laboratório Nacional de Luz Síncrotron, LNLS, Caixa Postal 6192, 13083-970 Campinas, Brazil

A. Traverse
LURE–Université Paris–Sud, 91405 Orsay Cedex, France
(Received 25 June 1999; revised manuscript received 14 October 1999)

This paper reports on the structural properties of Co_xFe_{1-x}/Ag discontinuous multilayers with $x = 0$, 0.3, 0.7, and 1. The evolution of the structural properties has been investigated by x-ray diffraction and x-ray-absorption spectroscopy (XAS). Thermal treatments for 10 min at temperatures ranging between 200 and 800°C, lead to breakup of the layers forming a heterogeneous alloy with magnetic clusters embedded in a metallic Ag matrix. The as-deposited Co/Ag presents a high compressive stress, while a slight tensile stress is observed in every other composition. After annealing there is a relaxation of the stress as well as a crystallographic ordering of the magnetic clusters. It is found from XAS measurements that, for the alloys with $x = 0.3$ and 0.7, there is a better-ordered structure around Co than Fe absorbing atoms. We conclude that Co atoms are within the core of the magnetic clusters, while Fe atoms occupy preferentially the interfacial positions near Ag. Co atoms in Co/Ag multilayers have a fcc structure.

I. INTRODUCTION

Magnetic thin films and multilayers have attracted considerable interest because of their peculiar properties, specifically for production of new magnetic materials for recording media and head sensors. In particular, the giant magnetoresistance (GMR) effect has attracted most of the interest not only in multilayered systems but also in granular heterogeneous alloys.[1,2] These later systems are usually obtained by cosputtering of two immiscible metallic elements or by sputtering of a metastable alloy: one is a ferromagnetic transition metal, and the other is a nonmagnetic transition metal or an insulator. These films generally are submitted to post-deposition annealing for further improvement of their properties. The role of annealing on the structural evolution of the granular films has been studied, and described by Cowache *et al.*[3] The thermal treatment induces a modification of the shape and size of the magnetic precipitates starting from a filamentary or dendritic to a more compact granular shape.

Another way to obtain a granular system was suggested by Hylton *et al.*[4] Starting from a multilayer structure with thin magnetic layers, and through post-deposition annealing, a breakup of the layers is obtained, resulting in a regular granular magnetic network embedded in a nonmagnetic matrix.

Independently of the way the granular system is obtained, one of the most important properties to be studied is certainly the atomic structure. The knowledge of the structure can help us to understand several related microscopic and macroscopic characteristics in the magnetotransport of these granular systems. For instance, an increase in GMR was observed when a small amount of Fe is added to Co in the Co/Cu multilayers.[5] However, the role played by the addition of Fe into Co is not well understood. From the preceding discussion it is evident that the study of the structure of the magnetic component is of fundamental importance for understanding the physical properties of these systems.

To determine the implications of the atomic structure on the physical properties of such systems, a technique more sensitive to short-range order is required for detailed investigations, especially due to small dimensionality of such systems. Thus, in complement of x-ray diffraction technique (XRD), the x-ray absorption spectroscopy (XAS), is an adequate technique for structural studies of systems that do not present long-range order.[6] While the XRD reveals information on the average structure of the film components, in the XAS technique the kind of probe atom can be selected and the local structure around each atom is possible to be obtained. Many examples of application of this technique can be found in the literature.[7,8]

The influence of the phase and a phase change from fcc to bcc on magnetic properties has been systematically investigated by Kubinski *et al.*,[9] who followed the structural evolution of films with epitaxial ferromagnetic precipitates in an Ag matrix grown epitaxially on MgO(100) substrates, such as Ag-X ($X = Co, Ni, Co_xNi_{1-x}, Co_xFe_{1-x}, Cu_xNi_{1-x}$) alloys; furthermore, a mixture of hcp Co, fcc Co, and stacking faults have been found for Co/Ag multilayers.[10] In the case

of the binary alloys any theoretical investigations from first principles have been performed.[11–13] Other authors have found a large decrease in the GMR as the crystal structure changed from fcc to bcc as in the case of Cu/Fe_xCo_{1-x} multilayers.[14]

This paper reports on the structural evolution of Co_xFe_{1-x} nanometric magnetic component obtained from Co_xFe_{1-x}/Ag discontinuous multilayers after thermal annealing. The evolution of the magnetic clusters after each thermal treatment was performed using the XRD and XAS.

II. EXPERIMENT

The $\{[Co_xFe_{1-x}(15\ Å)/Ag(50\ Å)]_{25}/Ag(50\ Å)\}$ multilayers, with concentrations of $x=0$, 0.3, 0.7, and 1, were prepared at room temperature by alternate deposition in an ultra-high vacuum dual *e*-beam evaporator. Commercial oxidized Si(111) wafers were used as substrate. All films were prepared with a deposition rate of 1 Å/s, controlled by a quartz microbalance. The total thickness of the films was 1650 Å. To have the exact composition of $x=0.3$ and 0.7 at the substrate, the Co_xFe_{1-x} alloys with suitable composition were prepared considering the differences in the volatility of the constituents.[15] The thickness of the Ag and Co_xFe_{1-x} layers were chosen to give an overall composition of 20 at. % for the ferromagnetic metal.

After deposition the films were annealed for 10 min at temperatures ranging from 200 to 800 °C in a vacuum furnace at a pressure better than 10^{-7} mbar. After all thermal treatments, the films were cooled down to room temperature for subsequent analysis.

The XRD measurements are performed in a θ-2θ Bragg-Brentano geometry at room temperature using Cu $K\alpha$ radiation ($\lambda=1.5406$ Å), on a conventional Rigaku DM 200 diffractometer. The x-ray residual stress analysis (XRSA) was accessed through asymmetric geometry using the two-exposure method, $\sin^2\omega$ plot, where ω is the sample tilt angle around the θ axis.[16,17] The residual stress is expected to lead to a linear dependence of the interplanar spacing, *d*, on $\sin^2\omega$, and it can be obtained from the slope of this plot. It is based on the change in the diffraction angle determined by the intensity maximum of a suitable reflection of the sample when it is placed consecutively with its surface at two different angles for the same diffracting plane. The intensity data was corrected considering the absorption and Lorentz-polarization factor.[17,18] The Si reflection of the substrate was used as internal standard to obtain the correct peak position, before each measurement.

The XAS measurements were obtained in two energy regions: the near edge structure (XANES) and the extended fine structure (EXAFS). XAS measurements have been performed around the Co and Fe *K* edges (7709 eV and 7112 eV) respectively, at the Laboratório Nacional de Luz Síncrotron, with energy steps of 0.8 eV for XANES and 2 eV for EXAFS modes and 2*s*/point. Two scans were added to obtain a better signal-to-noise ratio. The incident beam was collimated by slits and monochromatized with Si(111) crystals,[19] and its intensity measured by an ionization chamber. The data were collected in total electron yield in He atmosphere at room temperature.[20] Reference spectra of the bcc Fe and hcp Co foils were also measured for comparison and data analysis purposes. All spectra presented here were measured with the x-ray beam polarization vector in plane of the samples.

It is well established that XANES spectrum gives information on the local atomic structure around the absorbing atom and it may be used qualitatively as a fingerprint of the crystallographic structure by comparing the spectrum of known reference with XANES profiles of the samples.

The EXAFS spectra were analyzed by standard procedures, using the WINXAS software package.[21] It involves a background subtraction by means of a polynomial function normalized to the height of the absorption edge step. The various neighboring shells were obtained by a Fourier transform (FT) of the EXAFS signal, $\chi(k)$, in the wave-vector region ranging from 3 to 12.5 Å, using a Bessel window with a coefficient of 4. The inverse Fourier transform into *k* space of the EXAFS contribution corresponding the first-nearest-neighbor (NN) shell in the fcc structures, and the first and second NN shells in the bcc structures, were taken. Thus, structural parameters are obtained from least square fitting using experimental phase and amplitude functions, extracted from the Co reference spectrum when fcc structures are fitted. On the other hand, calculated phase and amplitude function from FEFF code[22,23] are used when bcc structures are fitted.

III. RESULTS AND DISCUSSION

The XRD patterns for all samples are shown in Fig. 1, and the reflection planes are indicated by the arrows. No satellites corresponding to the layered structure were observed in the spectra of the as-deposited samples, indicating a discontinuity of the magnetic layers and a roughness of the interfaces. Annealing at temperatures until 400 °C does not change significantly the XRD patterns, which are very similar to the ones for the as-deposited samples. For simplicity, only the spectra of as-deposited and annealed samples at 500 and 800 °C are exhibited in the figure.

As can be observed from the figure, the magnetic layer grows in a bcc structure for the Fe/Ag, $Co_{0.3}Fe_{0.7}/Ag$, and $Co_{0.7}Fe_{0.3}/Ag$ multilayers [Figs. 1(a)–1(c)] and in a fcc structure for the Co/Ag multilayer [Fig. 1(d)]. The second peak in the spectra corresponding to a bcc structure is a superposition of the Ag(200) and $Co_xFe_{1-x}(110)$ reflections. For annealed samples [Figs. 1(b) and 1(c)] when the cobalt concentration increases in the alloy, there is a decrease in the lattice parameter,[24] and a consequent decreasing in intensity of the second peak due to decrease of the overlap between the Ag(200) and $Co_{0.7}Fe_{0.3}(110)$ reflections. The peak of the $Co_{0.7}Fe_{0.3}(110)$ [Fig. 1(c)] can be slightly distinguished for annealed samples at 800 °C. As the annealing proceeds, the Ag lines sharpen and shift towards the bulk positions, and the magnetic phase displays an overall improvement of the crystallinity.

When the magnetic layers grow with a fcc structure, as in the case of Co/Ag films [Fig. 1(d)], the (111) orientation is preferred. The second peak in this spectrum corresponds to a superposition of both Ag(200) and Co(111). Magnetic layers for the as-deposited multilayer have a very disordered structure, indicating a relatively poor crystallinity. After annealing they undergo a structural evolution, which leads to nar-

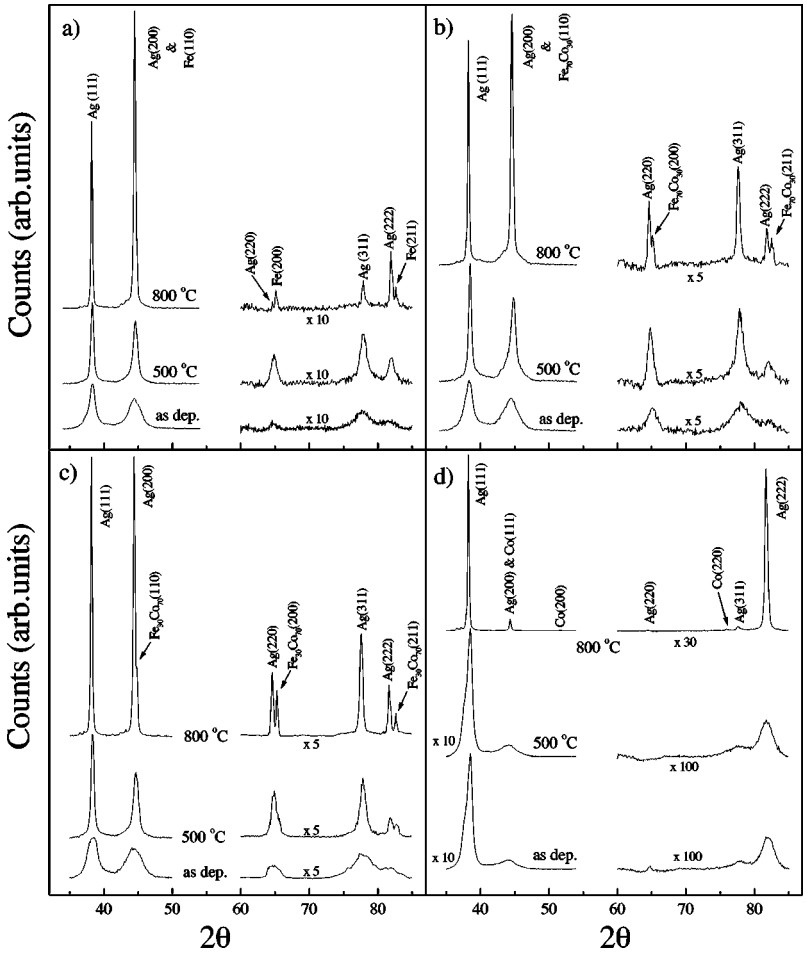

FIG. 1. θ-2θ XDR patterns for (a) Fe/Ag, (b) $Co_{0.3}Fe_{0.7}$/Ag, (c) $Co_{0.7}Fe_{0.3}$/Ag, and (d) Co/Ag. The diffraction planes are indicated by the arrows in the figure.

rowing of the peaks and an increase of the amplitude. As a consequence of the overlapping of the Ag(200) and Co(111) reflections the ordering temperature of the magnetic phase cannot be precisely estimated. Moreover, other reflections of the magnetic phase are visible, and a substantial increase of the Ag(111) and (222) peaks is observed when compared with the intensities of the other reflections, confirming the highly $\langle 111 \rangle$-textured direction of the Co/Ag samples.

The Ag(111) reflection in the Co/Ag as-deposited sample [Fig. 1(d)] splits into two overlapping lines, which can be identified by the shoulder at the low-angle part and by a more intense peak at the right-side part of the whole reflection. The lower-angle peak was assigned to a stress in the Co/Ag interface.[8] The stress in a thin film is usually divided into two major categories: thermal stress and intrinsic stress.[25] The thermal stress results from the difference in thermal-expansion coefficients between the film and the substrate. The intrinsic residual stresses are associated with the nucleation and growth mechanisms of the film, as well as with the interfacial relations between lattice parameter of the different constituent of the film.[15]

The XRSA assumes a biaxial stress field in the volume measured by XRD. The stress can be estimated from the following equation:

$$\sigma = \frac{\Delta d}{d_0} \frac{1}{\sin^2 \omega} \frac{E}{(1+\nu)}, \tag{1}$$

where $\Delta d/d_0$ is the relative change in the d value, ω is the tilting angle of the sample ($\omega = 0°$ is the symmetrical geometry), E is the Young's modulus, and ν is the Poisson ratio. Thus, the stress can be calculated directly from the slope of the least-square line fitted to the experimental data, assuming a linear relation between d and $\sin^2 \omega$, provided that Young's modulus and the Poisson ratio are known. The signal of σ define the type of stress, compressive for $\sigma < 0$ and tensile for $\sigma > 0$.

The results of the XRSA relative to the Ag(111) reflection line are shown in Fig. 2. The values were evaluated in terms of Eq. (1) using for Ag, $E = 7.58 \times 10^{10}$ N/m^2 and $\nu = 0.38$. For the as-deposited samples there is a slight tensile stress ($\sigma > 0$) for the films where the magnetic phase has a bcc structure (Co_xFe_{1-x} for $x = 0$, 0.3, and 0.7). In contrast, when the magnetic phase has a fcc structure,[8] pure Co, a rather high compressive stress ($\sigma < 0$) is observed. These changes are closely related with interfacial mismatch between different layers and the difference of the crystalline structures. These results can be attributed to the difference of the surface free energy between the Ag and the magnetic metals.[26] Because the origin of internal stress can be attributed to several factors,[25] we cannot determine precisely what is the origin here. After thermal treatment, the internal stress is relaxed. The same tendency is found for all samples. A small reduction of the stress is observed for Co_xFe_{1-x}/Ag for x ranging from 0 to 0.7 at. %; in contrast a substantial reduction of the stress occurs for Co/Ag.

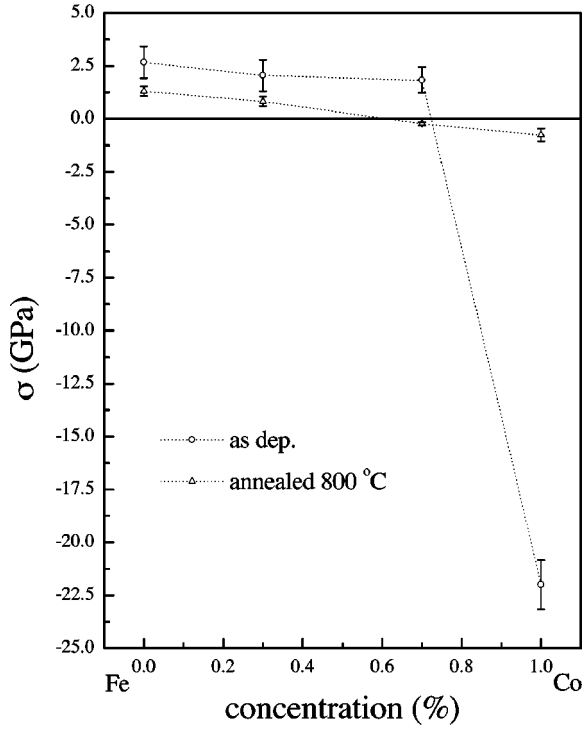

FIG. 2. Stress measurements for the Ag(111) reflection, as function of Co concentration for as-deposited and annealed samples at 800 °C.

Normalized XANES spectra of all samples are shown in Figs. 3–6. The spectra of the polycrystalline reference (bulk), Fe and/or Co foil, are given for comparison. For all spectra, the zero energy was chosen as the first inflection point of absorption with respect to photoelectron energy of the metallic edge (7112 eV for the Fe *K* edge and 7709 eV for the Co *K* edge). The bcc symmetry in pure Fe is characterized by a two-peak structure labeled A_1 and a smooth structure labeled A_2. Three peaks labeled B_1, B_2, and B_3 are characteristic of the hcp and fcc symmetry. The data for all edges in the figures are plotted on the same energy scale. The upper spectra are shifted vertically for clarity.

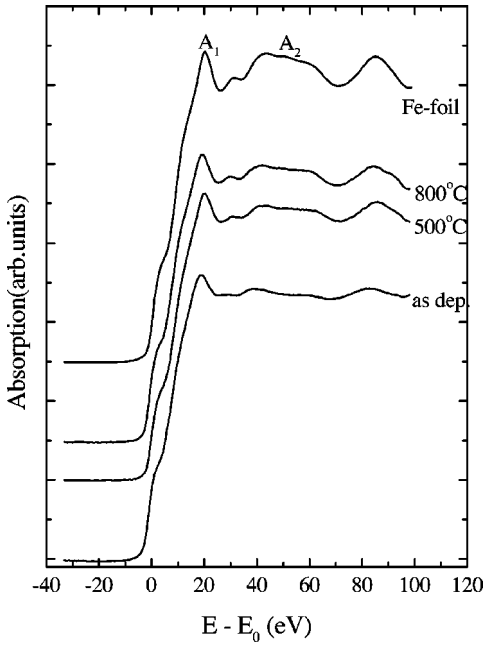

FIG. 3. Fe *K* edge XANES spectra for Fe/Ag as-deposited, and some annealed samples. The Fe reference spectrum is shown for comparison.

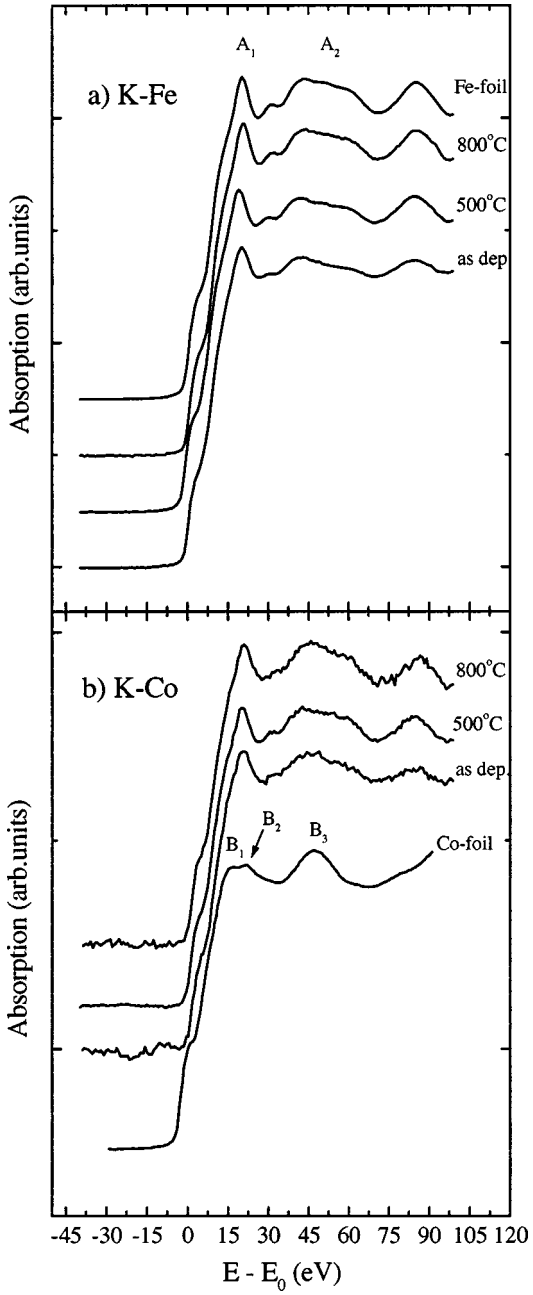

FIG. 4. Fe (a) and Co *K* edges (b) XANES spectra for $Co_{0.3}Fe_{0.7}$/Ag as-deposited and some annealed samples. The Fe reference spectrum is shown for comparison.

Fe *K* edge XANES spectra measured for the as-deposited and annealed Fe/Ag multilayers are shown in Fig. 3. Comparing the features of the spectra as-deposited Fe/Ag sample with the bcc reference Fe we see that all shapes are very similar, while overall amplitudes are smeared out indicating a poor crystalline order. These features do not change significantly until annealing at 400 °C. After annealing at high temperatures, namely, 500 and 800 °C, the shapes of the peaks show a structural evolution towards the structure of the

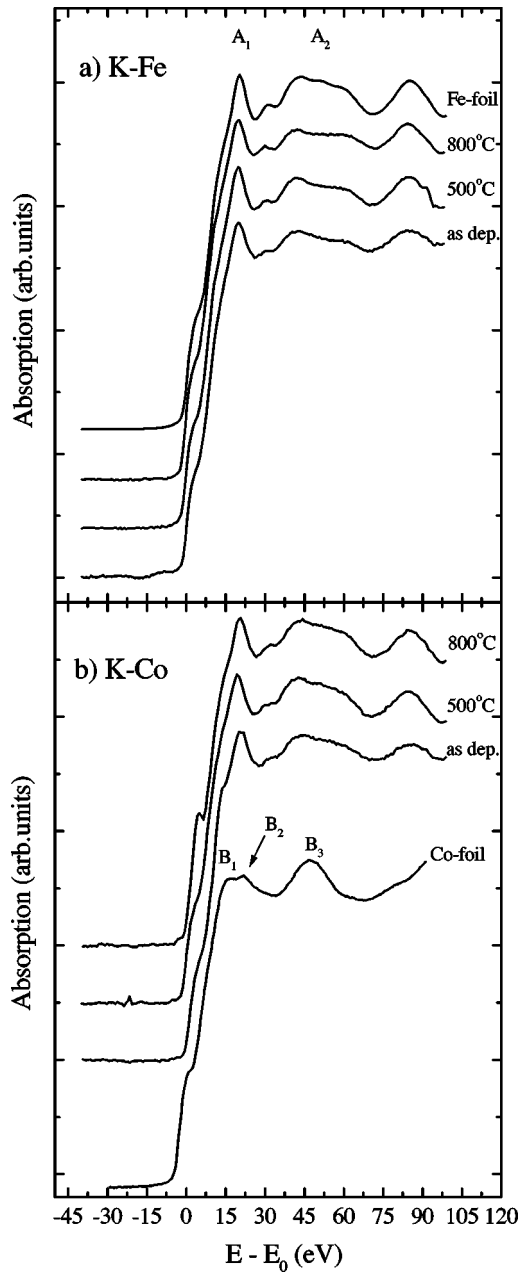

FIG. 5. Fe (a) and Co *K* edges (b) XANES spectra for $Co_{0.7}Fe_{0.3}$/Ag as-deposited and some annealed samples. The Fe reference spectrum is shown for comparison.

bcc reference Fe foil. The structure of the Fe in the Fe/Ag multilayered films is thus bcc, starting with a poor crystallinity for as-deposited sample, and evolving with an improvement of the crystallinity after annealing, according to what was observed by XRD.

Fe *K* edge and Co *K* edge XANES spectra measured for as-deposited and annealed $Co_{0.3}Fe_{0.7}$/Ag multilayers are shown in Fig. 4. The Fe *K* edge XANES profiles in Fig. 4(a) show the same feature as the Fe/Ag. On the other hand, for Co *K* edge [Fig. 4(b)] the spectra exhibit oscillations slightly more defined, even for the as-deposited sample. This feature can be ascribed to a better crystalline order of the Co. The data indicate that the Co adopts a bcc structure, as can be seen by visual comparison with Fe reference, confirming as is expected, that the magnetic layer corresponds to an alloy

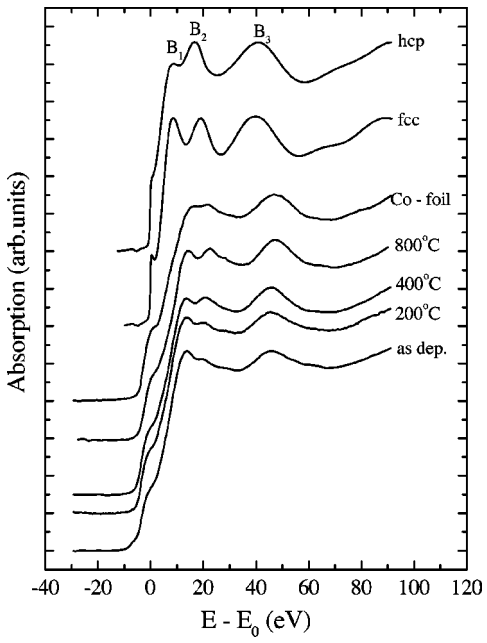

FIG. 6. Co *K* edge XANES spectra for Co/Ag as-deposited, and some annealed samples. The Co reference spectrum and simulations are shown for comparison.

of $Co_{0.3}Fe_{0.7}$. Comparing with XRD, we see that no isolated Co clusters are formed. It is important to note that despite the low concentration of Co atoms for this system, there is a better-ordered structure around Co-absorbing atoms than Fe atoms. This behavior can be explained assuming that the Fe atoms occupy preferentially the interfacial positions near Ag. This assumption is based on the fact that the Co atoms are insoluble in a Ag matrix, while the Fe atoms have a small solubility, as compared to the Co.

The previous observation is more evident in the $Co_{0.7}Fe_{0.3}$/Ag multilayers shown in Fig. 5. Although the Fe *K* edge XANES data reveal a local coordination geometry consistent with that of a bcc structure, a worse ordering can be seen even for upper annealing when compared with Fe reference, Fig. 5(a). Furthermore, the Co *K* edge XANES data also resemble very closely that of the Fe reference with a bcc structure, Fig. 5(b), although there is an improvement in the local atomic structure with annealing. The bcc ''fingerprint'' of the Co atoms in the Co *K* edge XANES in the $Co_{0.7}Fe_{0.3}$/Ag is clearly evidenced, although the occurrence of a bcc Co phase is not expected.[24]

Figure 6 shows Co *K* edge XANES spectra for Co/Ag multilayers for as-deposited and annealed samples. In the present system, it is not obvious to distinguish between a fcc and hcp structure for Co atoms, because the corresponding XANES spectra are quite similar. To tackle this question, simulations using FEFF code[22,23] for fcc and hcp Co have been performed, allowing us to differentiate between the two structures. The XANES spectra show an evolution with a clear difference between the features observed for the as-deposited sample and the one annealed at 200 °C, and those with upper annealing. As can be seen from the figure, there is a decrease in intensity of the peak B_1, while an increase in intensity is observed for the B_2 and B_3 peaks. A visible sharpening of the B_3 peak, reflecting a structural modification around Co atoms after annealing at 400 °C is also ob-

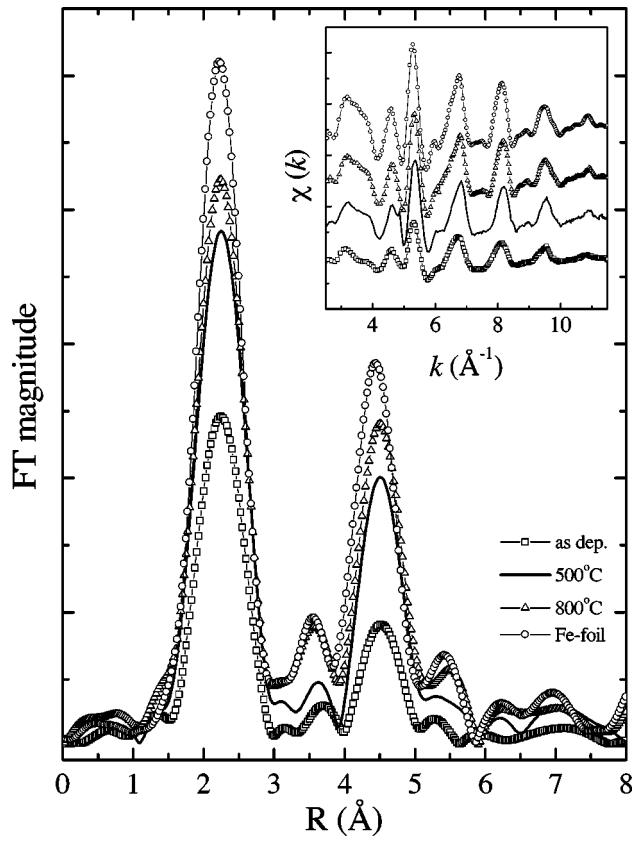

FIG. 7. Fe K edge Fourier transforms of EXAFS signals (inset) for Fe/Ag as-deposited, and some annealed samples. $\Delta k = 3 - 12.5$ Å, using a Bessel window with $\tau = 4$. The Fe reference spectrum is shown for comparison.

served. Furthermore, the XANES spectra are quite different from that of the Co reference. A comparison of the spectra of samples with the simulated ones provides an indication that the local coordination geometry of Co is consistent with a fcc structure.

The EXAFS oscillation[27] is expressed by the well-known formula

$$\chi(k) = \sum_j \frac{N_j f_j(k)}{kR_j} \sin[2kR_j + \phi_j] \exp\left[-2\left(k^2\sigma_j^2 + \frac{R_j}{\lambda_j(k)}\right)\right]. \quad (2)$$

It contains the structural parameters, the number of neighbor N_j, the near-neighbor distances R_j, and the Debye-Waller factor σ_j in the jth shell around the absorber. The magnitude of the backscattering amplitude is represented by $f_j(k)$; $\phi_j(k)$ is the total phase shift experienced by the scattered photoelectron, and $\lambda_j(k)$ is the mean-free path of the scattered photoelectron traveling from the absorbing atom to the backscattering in the jth shell.

The corresponding k^2 weighted Fourier transform (FT) magnitude of the Fe and Co K edges from the EXAFS signal (insets in the figures) are shown in Figs. 7–12. For comparison, the data are plotted together with FT of the references.

Figure 7 presents the FT of the Fe K edge EXAFS spectra for Fe/Ag as-deposited and annealed multilayer. When the spectra are compared with the reference, it is clear that the bcc local structure is preserved, but with a reduction in amplitude. The peak amplitudes increase with the annealing

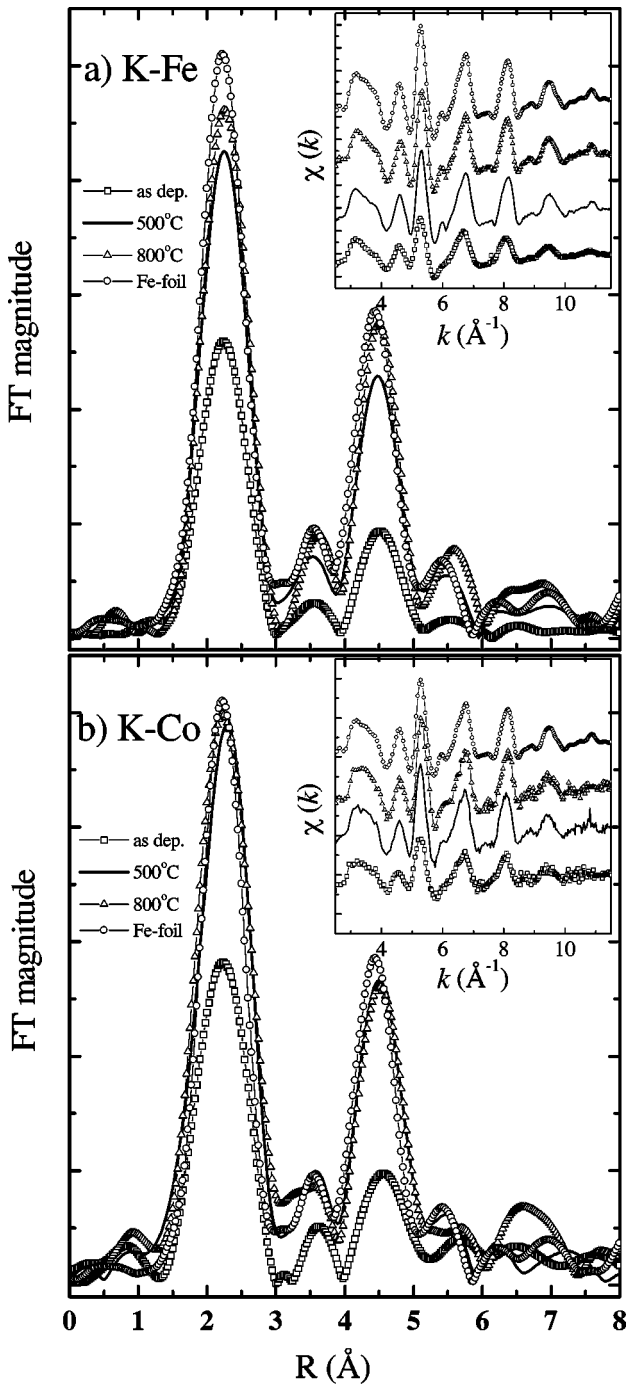

FIG. 8. Fe (a) and Co K edges (b) Fourier transforms of EXAFS signals (insets) for $Co_{0.3}Fe_{0.7}$/Ag as-deposited, and some annealed samples. $\Delta k = 3 - 12.5$ Å, using a Bessel window with $\tau = 4$. The Fe reference spectrum is shown for comparison.

temperature, which can be interpreted as an increase in the neighbor coordination for all shells. In order to obtain a quantitative estimate of structural parameters such as coordination numbers N, distances R, and Debye-Waller factor or disorder (due to both thermal and static disorder) σ, a simulation of the inverse Fourier transforms of the first peak has been performed. This peak is related to the first- and second-neighbor shells, therefore, due to proximity of the coordination spheres, the Fe reference cannot be used to analyze Fe-Fe interactions. Thus, the backscattering amplitude and the phase shift values were deduced from the EXAFS spec-

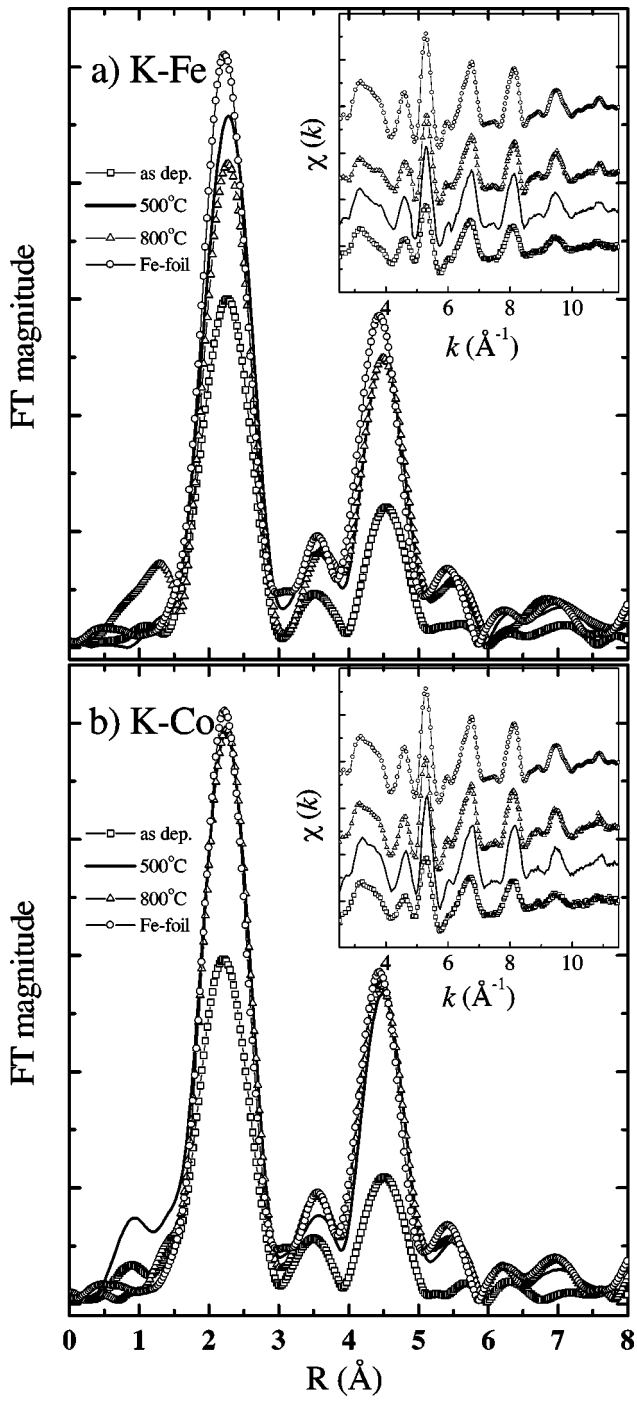

FIG. 9. Fe (a) and Co *K* edges (b) Fourier transforms of EXAFS signals (insets) for $Co_{0.7}Fe_{0.3}$/Ag as-deposited, and some annealed samples. $\Delta k = 3 - 12.5$ Å, using a Bessel window with $\tau = 4$. The Fe reference spectrum is shown for comparison.

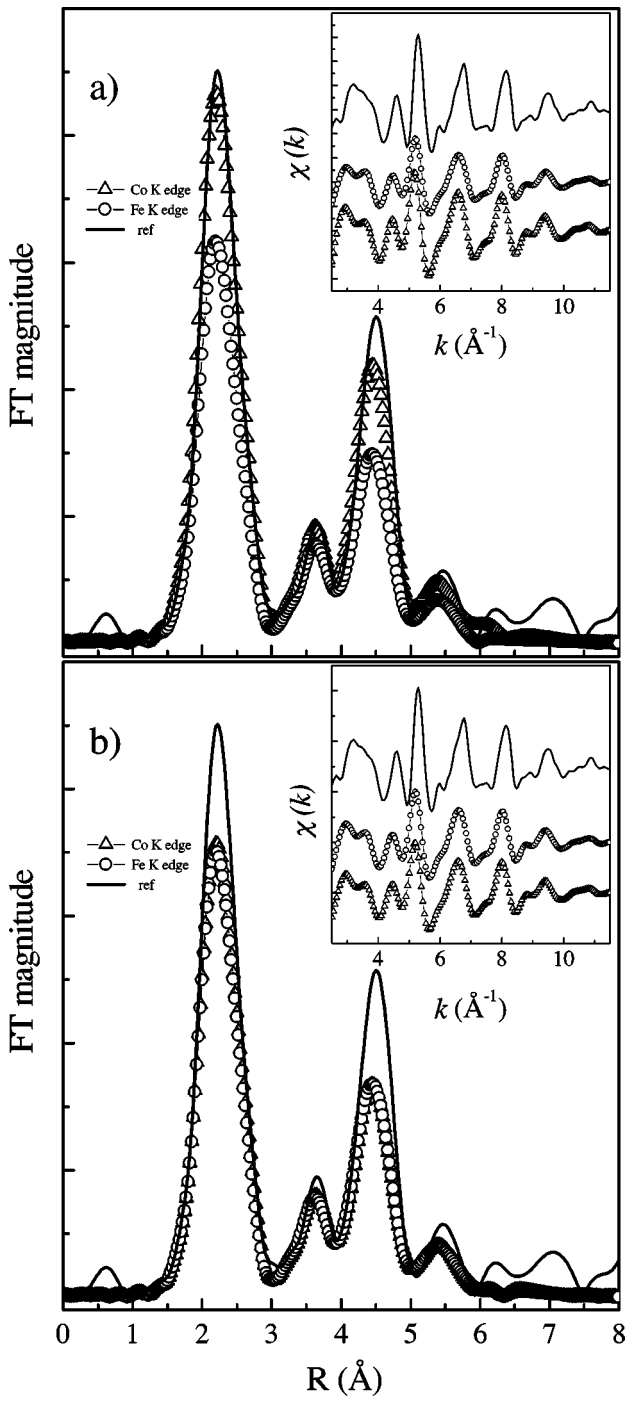

FIG. 10. Simulated Fe and Co *K* edges Fourier transforms and EXAFS signal (insets) for $Co_{0.3}Fe_{0.7}$: (a) cluster with Fe atoms at surface and (b) cluster with Fe and Co atoms in the surface. $\Delta k = 3 - 12.5$ Å, using a Bessel window with $\tau = 4$. Simulated Fe spectrum is shown for comparison.

trum of Co and from FEFF code.[22,23] The fit parameters are given in Table I and the uncertainties in the N, R, and σ were estimated at $\pm 10\%$, 0.01 Å, and $\pm 10\%$, respectively. As can be seen, the σ values are negative for every shell due to a relative disorder compared to that of the typical model compound from which backscattering amplitude and phase shifts were extracted.

The curve fitting, for two shells of neighboring atoms in the first peak, shows a reduced N and relatively high values of σ, indicating a disordered structure of the Fe. The samples show a better ordering as the annealing temperature increases, as is indicated by the increase of N and the decrease of σ. The distances of the first and second shells are very close to those expected for a bcc lattice. Finally, it is concluded that the local geometry of Fe in the Fe/Ag system is consistent with that of a bcc lattice, in agreement with previous results obtained by XANES and XRD.

The FT of the Fe and Co *K* edges EXAFS spectra, obtained from the as-deposited and annealed samples, of

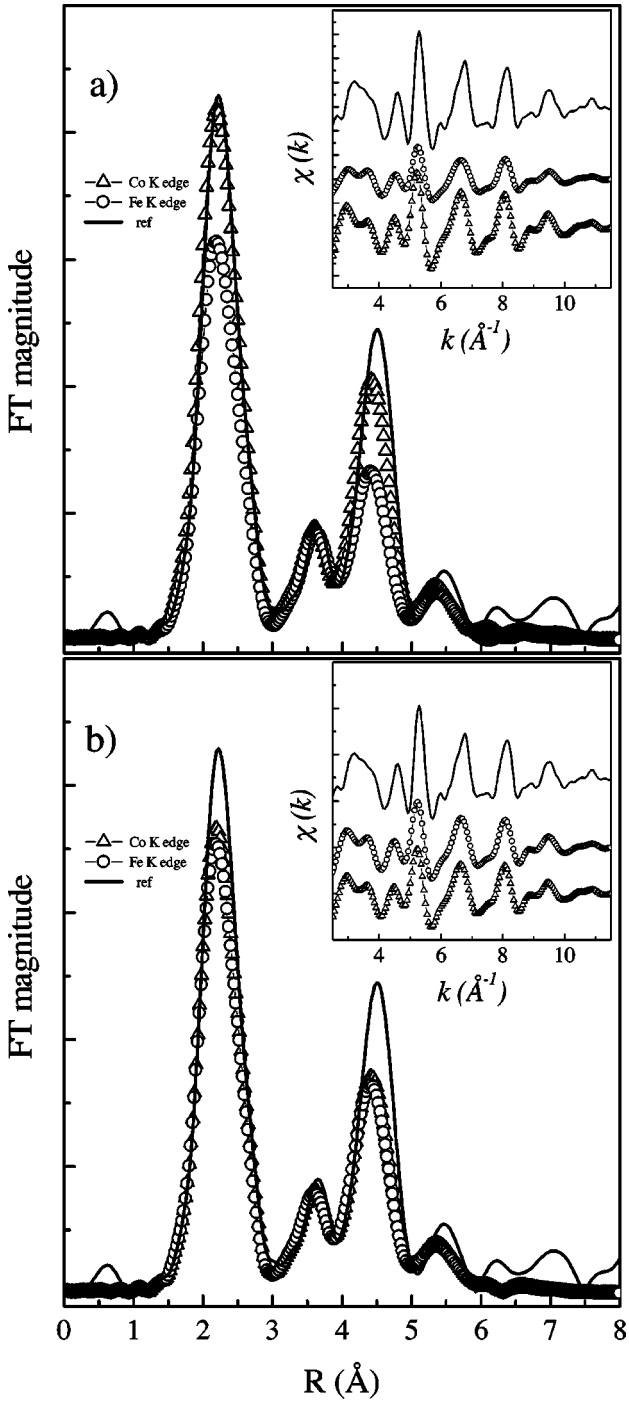

FIG. 11. Simulated Fe and Co K edges Fourier transforms and EXAFS signal (insets) for $Co_{0.7}Fe_{0.3}$: (a) cluster with Fe atoms at surface and (b) cluster with Fe and Co atoms in the surface. $\Delta k = 3 - 12.5$ Å, using a Bessel window with $\tau = 4$. Simulated Fe spectrum is shown for comparison.

$Co_{0.3}Fe_{0.7}$/Ag multilayers are shown in Fig. 8. The structures found are consistent with XANES results, where the Fe K edge EXAFS profiles [Fig. 8(a)] demonstrate a small amplitude when compared with the Co K edge EXAFS profiles [Fig. 8(b)]. These results are confirmed by the curve-fitting procedure described above. The fit results are listed in Table I. Comparing the N values of the Fe and Co edges, we see that the values for the Fe are smaller than that for the Co. These observations also suggest that the Fe atoms occupy the

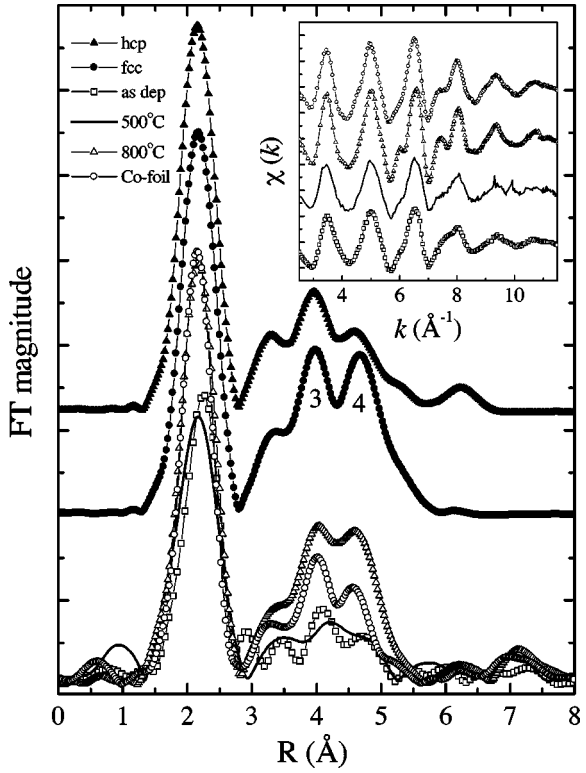

FIG. 12. Co K edge Fourier transforms of EXAFS signals (inset) for Co/Ag as-deposited, and some annealed samples. $\Delta k = 3 - 12.5$ Å, using a Bessel window with $\tau = 4$. The Co reference spectrum and simulations are shown for comparison.

interfacial positions of the clusters. On the other hand, the degree of structural disorder is nearly the same, as can be seen when the σ values are compared, see Table I. The R values for all samples are very similar, within the experimental uncertainty, and resemble those of the bcc structure.

It is noteworthy that the FT of the Fe and Co K edges for all as-deposited samples from $x = 0$ to 0.7 exhibit the same amplitudes, which are independent of the choice of the absorbing atom. This means that for the as-deposited films, the average ordering of the Fe and Co atoms is the same. On the other hand, after annealing the evolution, the FT amplitude is quite different for the Co than the Fe K edges. The amplitude in the Co K edge of the annealed samples recover the amplitude of the Fe reference, while the Fe K edge amplitude does not. These results indicate that Fe atoms should occupy the superficial positions of the magnetic clusters, as suggested above. In order to aid our interpretation of the FT EXAFS data, theoretical EXAFS data relative to Co_xFe_{1-x} alloys were generated using the FEFF code.[22,23] In this case, the clusters were generated with a bcc structure for Co_xFe_{1-x} alloys with two distinct configurations, one with the Fe atoms occupying preferentially the superficial positions of the cluster, and another with Co atoms also occupying the superficial positions of the cluster. All simulations were performed with thermal disorder using the correlated Debye model of the FEFF code.

The total signal of the cluster derived by the FEFF code [see Eq. (2)], $\chi_{cl}(k)$, for Co and Fe edges, was defined by averaging each signal, $\chi_i(k)$, from the absorbing atoms in all positions of the cluster. Thus the total EXAFS signal of the cluster is given by

TABLE I. Parameters determined from fitting the first peak in the Fourier-filtered EXAFS spectra as a function of the annealing temperature, T_A. The phase shift and amplitudes were extracted from the Co compound and FEFF code, where N is the coordination number; R is the distance of nearest neighbors in Å, and $\Delta\sigma^2$ is the Debye-Waller factor relative to the model compound givin in Å^2.

Sample	T_A	N_1	R_1	$\Delta\sigma_1^2(10^{-3})$	N_2	R_2	$\Delta\sigma_2^2(10^{-3})$	$\chi^2(10^{-6})$
				Fe *K* edge				
	as dep.	4.7	2.47	5.6	3.1	2.89	7.2	12.9
Fe/Ag	500 °C	5.8	2.47	2.9	5.3	2.85	6.1	15.4
	800 °C	6.2	2.48	1.7	4.5	2.86	6	13.4
	as dep.	4.8	2.50	3.4	4.2	2.88	9.2	23.8
$Co_{0.3}Fe_{0.7}$/Ag	500 °C	6.6	2.48	3	3.9	2.88	3.8	4.9
	800 °C	6.3	2.49	2.7	5.5	2.88	4.5	9.7
	as dep.	5.7	2.49	4	4.7	2.89	10	2.9
$Co_{0.7}Fe_{0.3}$/Ag	500 °C	6.3	2.48	1.8	4.8	2.89	5.6	7.1
	800 °C	5.6	2.48	1.8	4.5	2.89	5.2	10.1
Fe	Ref.	8	2.48		6	2.86		
				Co *K* edge				
	as dep.	6	2.48	3.5	4	2.89	9.5	13.7
$Co_{0.3}Fe_{0.7}$/Ag	500 °C	8	2.49	2.1	5	2.88	4.7	16.9
	800 °C	8	2.47	2.2	5.2	2.90	4.2	6
	as dep.	6.1	2.49	4	4.3	2.89	12	7.8
$Co_{0.7}Fe_{0.3}$/Ag	500 °C	7.6	2.48	2.4	6	2.86	7.6	33.8
	800 °C	7.9	2.50	2.6	6	2.87	7.6	25.3
	as dep.	8.5	2.53	0.8				11.1
Co/Ag	500 °C	9.2	2.49	1.2				12.2
	800 °C	12	2.50	−0.3				2.2
Co	Ref.	12	2.50					

$$\chi_{cl}^{\alpha}=\frac{1}{N^{\alpha}}\sum_{i}\chi_{i}^{\alpha}(k)n_{i}^{\alpha}, \tag{3}$$

where the index i denotes the coordination sphere and α the type of atom (Co or Fe). The terms n_i^{α} and N^{α} represent the number of atoms of type α in the coordination sphere i and the total number of atoms of type α in the cluster, respectively.

The FT curves and signals, obtained from the EXAFS simulations generated by FEFF's code for Co_xFe_{1-x} alloys for the two cases, are shown in Figs. 10 and 11. The spectra and signal of a simulated Fe reference cluster, with same dimension, thermal disorder, and number of the atoms of the simulated Co_xFe_{1-x} clusters (lattice parameter of α-Fe), is shown for comparison. They allow us to illustrate the difference in the local environment, comparing the FT for each *K* edge (Fe and Co), when the Fe atoms are located preferentially at the superficial positions of the clusters [Figs. 10(a) and 11(a)], and when the Co atoms also occupy the superficial positions of the clusters [Figs. 10(b) and 11(b)]. The calculated FT curves for Co_xFe_{1-x} alloys for the two situations, clearly show that the occupation of superficial and inner sites differ appreciably over FT magnitude for Fe and Co *K* edges. The case where the Fe atoms are in the interfacial positions near the Ag is in conformity with the experimental observations. However, it is important to emphasize that these results are only qualitative, since for the simulations we adopt clusters spherically symmetric and with a limited number of atoms, due to FEFF restrictions. Thus, it is incorrect to compare quantitatively the difference in two edges between the simulations and the experimental observations.

The same scheme described above can be used to generate Co_xFe_{1-x} alloys with an ordered structure for both Fe and Co compositions. We have considered the Fe_3Al structure,[24] to generate the Fe_3Co and Co_3Fe, using the equilibrium lattice parameter obtained by Schwartz *et al.*[13] However, these ordered structures correspond to 25 and 75 at. % Co or Fe, which are slightly different from the compositions of our samples. To solve this problem, the phases have been considered as a partially ordered alloy with Fe_3Al structure with one sublattice fully occupied by the atoms with largest concentration, and the other sublattice randomly occupied by the remaining atoms.

The FT, not shown here, for both compositions exhibit a different magnitude for the Fe and Co *K* edges, with the FT magnitude more intense for *K* edge of the atom with smallest concentration. A different behavior of the FT magnitude is also observed when compared with the FT magnitude obtained for clusters with disordered structures, see Figs. 10 and 11. Thus, the simulations using clusters with disordered structures in which Fe atoms occupy interfacial positions appear to be more realistic than ordered ones.

Figure 12 displays the FT and the signals (inset) of the Co *K* edge EXAFS signal (inset) for the Co/Ag system. The figure also shows the simulation using FEFF code for hcp and fcc Co. Comparing the FT obtained experimentally with the simulation we see that the Co presents a fcc structure. This difference is evidenced by comparing the intensities of the peaks 3 and 4 with the simulated spectrum corresponding to the fcc Co, which are quite different from the FT obtained for the Co foil. There are no evidences of near-neighbor Co-Ag contribution, as was reported by Regnard *et al.*[7] for sputtered CoAg films. The amplitudes of the FT peak for the as-deposited sample is small when compared with the Co reference. This is an evidence of a reduction in the *N* for every shell. This effect disappears for high-annealing temperatures, where the intensity of the peaks are close to that of the Co foil, indicating an ordering of the Co structure. The curve fitting, with a single shell of neighboring atoms, indicates a reduction in *N* for the as-deposited and annealed samples until 500 °C. After annealing at 800 °C, an increase of *N* is observed, see Table I.

As reported by Tyson *et al.*,[28] a possible asymmetry in the in-plane and out-of-plane bond distances of Co-Co, Co-Fe, and Fe-Fe can be expected. Although, preliminary measurements have not shown any significant differences, a detailed study using both perpendicular and parallel polarizations is being performed and will be presented in the near future.

IV. CONCLUSIONS

The structural properties of the Co_xFe_{1-x}/Ag series of discontinuous multilayers exhibit a wide variety of interesting characteristics that depend upon the composition of magnetic layers and post-deposition annealing. It is important to emphasize that the as-deposited samples are formed by discontinuous magnetic layers separated by continuous Ag layers. After annealing at 400°C there is a breakup of the magnetic layers leading to a regular network of magnetic clusters imbedded in an Ag matrix.

For the as-deposited Co/Ag multilayers the Co layers assume a fcc structure being highly disordered and discontinuous with only a short-range order, as observed by XRD and XAS measurements. The Co/Ag interfaces have compressive stress due to the difference of the surface energies between the Ag and Co. This stress is responsible for the formation of islands of Co at the interfaces, which contributes for the roughness and discontinuity of the Co layers. The Ag layers present a high $\langle 111 \rangle$ texture that is enhanced after thermal treatment, due to the release of stress and defects. On the other hand, when the magnetic layers are composed of a $Co_{0.7}Fe_{0.3}$ alloy, there is a drastic diminution of the stress. The stress changes its sign, passing from a compressive to tensile stress with a low value, when compared with the as-deposited Co/Ag discontinuous multilayers. This magnetic layer adopts, as expected, a bcc structure that grows incoherently with the fcc Ag layer. Thus, a great number of dislocations should appear at the $Co_{0.3}Fe_{0.7}$/Ag interface releasing the stress. Increasing the Fe content in the alloy, for $Co_{0.3}Fe_{0.7}$/Ag, a little increase of the tensile stress is observed, reaching to 2.5 GPa for the Fe/Ag discontinuous multilayers. This difference can be due to the fact that adding Fe into Co will cause an enhancement of the wetness of the magnetic layer on Ag causing a tensile stress at the Ag interface. The thermal treatment reduces the stresses to small values. The reduction of stress is accompanied by a crystalline ordering independent of the composition of the magnetic layer according to the XRD, XANES, and EXAFS measurements.

It is interesting to note that FT transforms of the EXAFS spectra have the same amplitude for all the as-deposited samples, while for the annealed ones, some differences are observed. The FT for the Fe *K* edge for samples where the magnetic layers are formed by pure Fe or Co_xFe_{1-x} alloys does not recover the same amplitude of the Fe reference. On the other hand, after annealing, the Co *K* edges FT amplitudes for magnetic layers formed by pure Co or Co_xFe_{1-x} alloys recover the same value of the Fe reference. It means that the as-deposited samples have approximately the same disorder. After annealing the Co atoms seem to have a more symmetrical neighborhood than does the Fe atoms indicating that the latter occupy preferentially the superficial positions of the magnetic clusters in the alloys.

Simulated EXAFS data relative to Co_xFe_{1-x} alloys with disordered and partially ordered structures were generated using the FEFF code. EXAFS signals as well as the FT amplitudes obtained at the Co and Fe edges for clusters with a bcc disordered structure, in which the Fe atoms occupy preferentially the superficial positions, appear to follow the same trend observed experimentally for the Co_xFe_{1-x} granular alloys. We wish to stress that the simulations were performed using spherical clusters, without shape variation and size distributions, in which a limited number of atoms were used. Probably these are some of the limiting factors in the quantitative comparison of the FT magnitude in two edges between the simulations and the experimental observation.

ACKNOWLEDGMENTS

The authors wish to acknowledge the partial support of this work by CNPq, LNLS, CAPES, FINEP, FAPERGS, and FAPESP Brazilian financial agencies.

[1] A. Berkowitz, J.R. Mitchell, M.J. Carey, A.P. Young, S. Zhang, F.E. Spada, F.T. Parker, A. Hutten, and G. Thomas, Phys. Rev. Lett. **68**, 3745 (1992).

[2] J.Q. Xiao, J.S. Jiang, and C.L. Chien, Phys. Rev. Lett. **68**, 3749 (1992).

[3] C. Cowache, B. Dieny, S.R. Teixeira, and O. Redon, Phys. Met. Metallogr. **79**, 61 (1995).

[4] T.L. Hylton, K.R. Coffey, M.A. Parker, and J.K. Howard, Science **261**, 1021 (1993).

[5] K. Inomata and Y. Saito, J. Magn. Magn. Mater. **126**, 425 (1993).

[6] A. Traverse, New J. Chem. **22**, 677 (1998).

[7] J. R. Regnard, C. Revenant-Brizard, B. Dieny, B. Mevel, and J. Mimault, in *Metastable Phases and Microstructures*, edited by R. Bormann *et al.*, MRS Symposia Proceedings No. 400 (Mate-

rials Research Society, Pittsburgh, 1996), p. 329.
[8] W.H. Flores, S.R. Teixeira, J. Geshev, J.B.M. da Cunha, P.J. Schilling, A. Traverse, and M.C. Martins Alves, J. Magn. Magn. Mater. **188**, 17 (1998).
[9] D.J. Kubinski and H. Holloway, J. Appl. Phys. **77**, 782 (1995); **77**, 2010 (1995); **77**, 2508 (1995); D.J. Kubinski, H. Holloway, and J. Hangas, *ibid.* **77**, 3331 (1995).
[10] E.A.M. van Alphen and W.J.M. de Jonge, Phys. Rev. B **51**, 8182 (1995).
[11] P. James, O. Eriksson, B. Johansson, and I.A. Abrikosov, Phys. Rev. B **59**, 419 (1999).
[12] I.A. Abrikosov, P. James, O. Eriksson, P. Soderlind, A.V. Ruban, H.L. Skriver, and B. Johansson, Phys. Rev. B **54**, 3380 (1996).
[13] K. Schwarz, P. Mohn, P. Blaha, and J. Kübler, J. Phys. F **14**, 2659 (1984).
[14] H. Kano, Y. Iwasaki, K. Hayashi, and K. Aso, J. Magn. Magn. Mater. **126**, 445 (1993).
[15] M. Ohring, *The Materials Science of Thin Films* (Academic Press, San Diego, 1992).
[16] M. Leoni and P. Scardi, in *Thin Film Characterization by Advanced X-Ray Diffraction Techniques*, edited by G. Cappuccio and M. L. Terranova (SIS-Pubblicazioni, Frascati, 1996), p. 113.
[17] H. P. Klug and L. E. Alexander, *X-Ray Diffraction for Polycrystalline and Amorphous Materials*, 2nd ed. (Wiley, New York, 1974), p. 755.
[18] B. D. Cullity, *Elements of X-Ray Diffraction*, 2nd ed. (Addison-Wesley, Reading MA, 1978), p. 463.
[19] H. Tolentino, D.Z. Cruz, V. Compagnon-Cailhol, E. Tamura, and M.C. Martins Alves, J. Synchrotron Radiat. **5**, 521 (1998).
[20] G. Tourillon, E. Dartyge, A. Fontaine, M. Lemonnier, and F. Bartol, Phys. Lett. A **121**, 251 (1987).
[21] T.J. Ressler, J. Phys. IV **7**, C2-269 (1997).
[22] J.J. Rehr, R.C. Albers, and S.I. Zabinsky, Phys. Rev. Lett. **69**, 3397 (1992).
[23] J.J. Rehr, Jpn. J. Appl. Phys., Part 1 **32**, 8 (1993).
[24] Pearson, *Handbook of Lattice Spacing and Structures of Metals* (Pergamon Press, London, 1964).
[25] R. W. Hoffman, in *Physics of Thin Films*, edited by G. Hass and R. F. Thun (Academic Press, New York, 1966), Vol. 3, p. 211.
[26] *Handbook of Thin Film Technology*, edited by L. I. Maisser and R. Glang (McGraw-Hill, New York, 1983).
[27] See, for instance, D. C. Koningsberger and R. Prins, *X-ray Absorption Principles, Applications, Techniques of EXAFS, SEXAFS, and XANES* (Wiley, New York, 1988); B. K. Teo, *EXAFS: Basic Principles and Data Analysis* (Springer, Berlin, 1986).
[28] T.A. Tyson, S.D. Conradson, R.F.C. Farrow, and B.A. Jones, Phys. Rev. B **54**, 3702 (1996).